Neural Correlate and Movement Decoding of Simultaneous-and-Sequential Bimanual Movements Using EEG Signals

Jiarong Wang, Luzheng Bi, *Senior Member, IEEE*, Weijie Fei, Xiangyu Xu, Aixian Liu, Linhong Mo, and Aberham Genetu Feleke

Abstract— **Bimanual coordination is important for developing a natural motor brain-computer interface (BCI) from electroencephalogram (EEG) signals, covering the aspects of bilateral arm training for rehabilitation, bimanual coordination for daily-life assistance, and also improving the multidimensional control of BCIs. For the same task targets of both hands, simultaneous and sequential bimanual movements are two different bimanual coordination manners. Planning and performing motor sequences are the fundamental abilities of humans, and it is more natural to execute sequential movements compared to simultaneous movements in many complex tasks. However, to date, for these two different manners in which two hands coordinated to reach the same task targets, the differences in the neural correlate and also the feasibility of movement discrimination have not been explored. In this study, we aimed to investigate these two issues based on a bimanual reaching task for the first time. Finally, neural correlates in the view of the movement-related cortical potentials, event-related oscillations, and source imaging showed unique neural encoding patterns of sequential movements. Besides, for the same task targets of both hands, the simultaneous and sequential bimanual movements were successfully discriminated in both pre-movement and movement execution periods. This study revealed the neural encoding patterns of sequential bimanual movements and presented its values in developing a more natural and good-performance motor BCI.**

Index Terms— **Brain-computer interface (BCI), electroencephalogram (EEG), bimanual movements, motor sequence.**

I. INTRODUCTION

MOTOR rehabilitation and assistance are two vital aspects for individuals with motor deficits [1]. Motor rehabilitation training acts to restore impaired motor abilities via recovering injured brain functions or reorganizing brain function networks utilizing residual functions [2]. Motor assistance of daily life (ADL) can improve individuals' life independence by assisting motor functions in terms of degrees of freedom, range, and strength. For both motor rehabilitation and assistance, involving the individuals in an active way according to their motor intentions can benefit in enhancing neuroplasticity and allowing more usable and natural controls of peripheral devices. To decipher movement intentions, the non-invasive electroencephalography-based (EEG-based) brain-computer interface (BCI) is a promising tool [3]. It can detect motor intentions from scalp signals directly relying on the changes of motor-related potentials and oscillations [4].

Among EEG-based motor-BCIs, instead of inducing motor-related neural modulations based on repetitive visual or kinesthetic motor imagination (MI) [5], translating neural information associated with motor execution (ME) or motor attempt (MA) as control commands is a more intuitive and natural way, e.g., hand open-and-close attempts of the affected limb to control robotic hand for neuro-rehabilitation [6], and reach-and-grasp movements to control prosthetic limbs for ADL [7]. Prior studies have shown that the brain motor cortex encodes movement information of both unilateral and bilateral movements of limbs. For decades, discriminating unilateral movements, such as center-our reaching task [8], [9], has been well-explored. Brain activation patterns of different unilateral movements of limbs are characterized for neurophysiological visualization and interpretation, e.g., motor-related cortical potentials (MRCPs), event-related desynchronization or synchronization (ERD/S), brain connectivity network, etc. The decoded movement commands are used to control exoskeleton [10], prostheses [11], orthosis devices [12], and robotic gloves [6] for a reliable human-machine interaction. Impressive neuro-motor rehabilitation effects of affected limbs are observed in post-stroke patients [13].

Besides unilateral-limb movements' decoding, discriminating bilateral-limb movements from EEG signals is of great value, which mainly lies in three aspects. First, previous studies reported the positive motor recovery effects and

neuroplastic benefits of bilateral arm training (BAT) over hemiplegic patients [14]. For symmetric BAT, the patients are required to perform consistent actions using both unaffected and affected limbs for synchronous training, e.g., raising both arms, and grabbing with both hands, and for asymmetric BAT, the patients are required to perform inconsistent actions for coordination training, e.g., tying a knot and zipping. Simultaneous bilateral motor activities can enhance neural activation of the ipsilesional hemisphere and alleviate interhemispheric inhibition. Second, bilateral coordinating movements of both arms and hands are necessary for activities in daily life [15], such as dressing and undressing, and twisting the lid off the bottle. Third, compared to increasing movement types of unilateral limb, involving bilateral-limb movements to be discriminated from unilateral movements can improve multi-dimensional control and meanwhile maintain well decoding performance, which can be attributed to the distinct brain activation patterns of unilateral and bilateral movements [16].

In recent years, several studies have turned attention to the simultaneous bilateral movements' decoding from EEG signals, including bimanual center-out movements [17], [18], bimanual reach-and-grasp movements [15], and bimanual cyclical tasks [19]. Actually, humans can perform tasks with two hands either simultaneously or sequentially. Though some tasks can be performed by two hands simultaneously, many natural tasks involve a sequence of bilateral movements. For example, if the patients want to pour water into a cup to drink, they would complete the tasks of pouring water into the cup, lifting the cup, and drinking water in sequence, instead of completing them concurrently. Planning and executing complex sequential movements is a fundamental motor-process ability of the human brain, and this motor skill requires the elaborate organization of serially ordered motor elements. For a motor sequence, our brain plans the full sequence as a task set before execution and holds it in working memory, rather than plans the next motor element separately after the last one is done [20].

Some previous studies have paid attentions to the EEG patterns and decoding of sequential movements. Yi et al. [21] designed a MI paradigm involving motor sequences of compound limbs to improve MI-BCI performance. Results showed that there were significantly larger ERD during imagination of multi-limb motor sequences than that of single limb. Seeber et al. [22] investigated the temporal relation between EEG oscillations and rhythmic finger-sequence movements. Phase-related amplitude modulations were observed during rhythmic finger movements, and large-scale networks were separated to research cortical sensorimotor system. To improve ERD during MI and classification accuracy, Bian et al. [23] introduced a MI paradigm of complex motor tasks (playing part of a piano tune) with dynamic video guidance. Though these studies showed the neural patterns of motor sequences and the feasibility to decode them, bimanual sequential coordination movements are not considered. Comparing the neural patterns of bimanual sequential movements with other bimanual coordination movements and research the feasibility to discriminate them from EEG signals would contribute to the bimanual motor-BCIs.

Supposing there are two reaching targets for two hands, a person can reach them either simultaneously or sequentially. However, the differences in brain activation patterns between the simultaneous and sequential bimanual movements remain unclear. In addition, considering that the brain can plan the simultaneous and sequential bimanual movements before motor initiation, whether it is feasible to discriminate the planned bimanual movements from the working memory needs to be explored. Here, we aim to investigate the neural correlating and movement decoding of simultaneous-and-sequential bimanual movements based on a bimanual reaching task for the first time. The findings surprisingly revealed the unique motor-related neural encoding patterns of sequential bimanual movements compared to simultaneous bimanual movements. Furthermore, the simultaneous and sequential bimanual movements were successfully discriminated in the pre-movement period. This study is ponderable for developing a more natural motor-BCI involving sequential bimanual movements and can facilitate the motor-BCI to be applied in both bilateral neuro-rehabilitation training and daily-life assistance.

II. METHODS

A. Participants

Nine right-handed healthy subjects (4 women and 5 men; mean age 24 years) participated in the experiment. This study was conducted at the Beijing Institute of Technology, Beijing, China, and it was approved by the Local Ethics Committee of the Beijing Institute of Technology (approval number: BIT-EC-H-2023016). All subjects were informed of the consent form before the experiment, and the experiment adhered to the Declaration of Helsinki.

B. Experimental Procedure

The experimental paradigm is illustrated in Fig. 1 (a). During the experiments, the subjects were seated in a comfortable chair with both hands put on a table. The experiment includes 5 blocks of the unimanual, simultaneous bimanual, and sequential bimanual horizontally outward reaching movements. For the unimanual movements, the subjects were required to move their left or right hand in horizontally-outward directions (left or right) while keeping the opposite hand still. For the simultaneous bimanual movements, the subjects were required to move both left and right hands outwards simultaneously. For the sequential bimanual movements, the subjects were required to execute a sequence of left hand first and then right hand movement, or vice versa. For each sequence, when the first movement element was completed, the second movement element had to be executed as soon as possible. The experiment contained 5 blocks corresponding to 5 different movement types, and each block consisted of 8 runs. There were 10 trials in each run. Therefore, we could collect 80 trials for each movement type. Different runs of different blocks were conducted randomly for order balance.

The timeline of one trial is depicted in Fig. 1 (b). For each trial, it lasts for 14 s, including 3 s for rest, 3 s for movement preparation, 4 s for movement execution, and 4 s

for relaxation. When one trial started, there was nothing on the screen. At the third second, one arrow with a dotted line is shown on the screen, indicating the hand and its movement direction to be executed. At the sixth second, one arrow with a solid line is shown, indicating the subjects to execute the movements immediately. The red and blue colors of the arrows correspond to the left and right hands, respectively. For the unimanual movements, a single arrow appears. For the simultaneous bimanual movements, two arrows appear at the same time. For the sequential bimanual movements, two arrows appear sequentially with an interval of 500 ms. Noting that the sequential arrows only appear for the preparation cue, and they also appear simultaneously for the go cue to ensure that the sequential information is only encoded in the working memory period. During the experiment, the subjects could take a rest whenever they requested.

C. Data Collection and Preprocessing

EEG data were recorded using a 64-channel amplifier (Neuracle, China) sampled to 1000 Hz. Thirty-two electrodes were mounted according to the 5% international 10/20 EEG system (see Fig. 1(C)). Two extra electrooculogram (EOG) electrodes were positioned at the outer canthi of both eyes. Electrode impedances were kept below 5 kΩ. Each position sensor (Fastrack) was fixed to one hand to collect its position in three-dimension space at a sampling rate of 50 Hz.

After data was collected, position data was filtered using a 4-order Butterworth filter at a band of [0.02 4] Hz to remove noise caused by the tremors of hands. The movement onset points of each trial were labeled by the velocity of hand movement with a threshold of 1 cm/s. The movement onset was used to align the EEG signals. EEG signals were down-sampled to 100 Hz. Baseline correction with the sliding window was applied to suppress drift. Independent component analysis (ICA) was used to reject independent components whose correlation coefficient with EOG signals was above 0.4. Artifact subspace reconstruction (ASR) was applied to remove large-amplitude movement artifacts. Common average reference filter was applied to eliminate the common background noise. After that, the EEG data flow was segmented into trials with [−6, 6] s of movement onset, and the trials whose amplitude exceeds the threshold of ±100 μV were rejected. Since electromyogram (EMG) artifacts are mainly in band of 20-300 Hz, and we mainly focused on the low-frequency band of EEG signals, no more EMG artifacts were corrected.

D. Neural Correlating

1) Movement-Related Cortical Potentials (MRCPs): The MRCPs were plotted to inspect the motor-related signal potentials in the low-frequency temporal band. In this work, we first extracted the low-frequency temporal components from each trial using a 4th-order [0.01, 4] Hz Butterworth filter and then averaged all trials of each movement type across all subjects.

2) Event-Related Spectral Perturbation (ERSP): To compare the task-related spectral power changes, the ERSP was used to map event-related power desynchronization/synchronization in the time-frequency domain. The changes of ERSP across

trials were computed as follows:

$$ERSP(t, f, c) = \frac{1}{N} \sum_{n=1}^{N} |TFR_n(t, f, c)|^2, \tag{1}$$

where $TFR_n(t, f, c)$ denotes the spectral power estimation of the nth trial at time t, frequency f, and electrode c. N is the number of trials of each movement type. The ERSP was baseline-normalized to the period of $(-6, -4.5)$ s during rest, and mapped in the frequency band of [0, 40] Hz. In this work, the spectral perturbation was estimated by using *newtimef* function of EEGLAB toolbox in MATLAB [24].

3) EEG Source Analysis: To observe the brain activation patterns in the source space, we mapped the EEG data from the sensor level to the source level by using the source imaging technique. We first established a forward head model to obtain the propagation patterns of electrical fields from the cortex to the scalp. The head model was established by co-registering the ICBM152 boundary element model (BEM) with recorded EEG electrodes using open source software Brainstorm. The conductivities of the scalp, skull, and brain layers of BEM were set to be 1, 0.0125, and 1, respectively. The forward model was estimated using OpenMEEG BEM [25] in the source space of the cortex surface. Then, we computed the inverse estimation of brain sources using sLORETA with unconstrained dipole orientations and the minimum norm imaging method [26].

E. Movements' Decoding

To decode movements while keeping the decoding models with good interpretability, we applied a discriminant manifold learning method for feature dimension reduction and used the linear discrimination analysis (LDA) for classification. First, the features of MRCPs were extracted as input. Then, the low-dimensional sub-manifold was built using a nearest neighbor graph embedding to reduce the feature dimension. Finally, LDA was applied to discriminate sub-manifold feature maps for movement decoding.

To extract MRCP information, we selected the temporal amplitudes from the low-frequency band of [0.01, 4] Hz and 32 electrodes as features. The length of decoding window was 1 s and the sampling rate was 100 Hz. For each trial, the amplitudes were reshaped into a one-dimensional feature vector (100×32).

To reduce the feature dimension, we introduced the locality sensitive discriminant analysis (LSDA) method, which could discover the intrinsic geometrical structure of the underlying data manifold [27]. The work by Lin et al. [28] showed the superiority of LSDA in decoding performance. Besides, as a manifold-leaning method, LSDA could discover the intrinsic geometrical structure of the underlying data manifold and also has the advantages of interpretability and simple computation. Thus, in this work, we applied LSDA to reduce the feature dimension to 50. Given the EEG data sample $\mathbf{X} = \{\mathbf{x}_i\}_{i=1}^{N} \in \mathbb{R}^{N \times M}$, where N is the number of samples, and M is the number of feature points, it is supposed that there is an underlying sub-manifold $\mathcal{L}$ of data. The local geometrical structure of sub-manifold $\mathcal{L}$ can be modeled by a
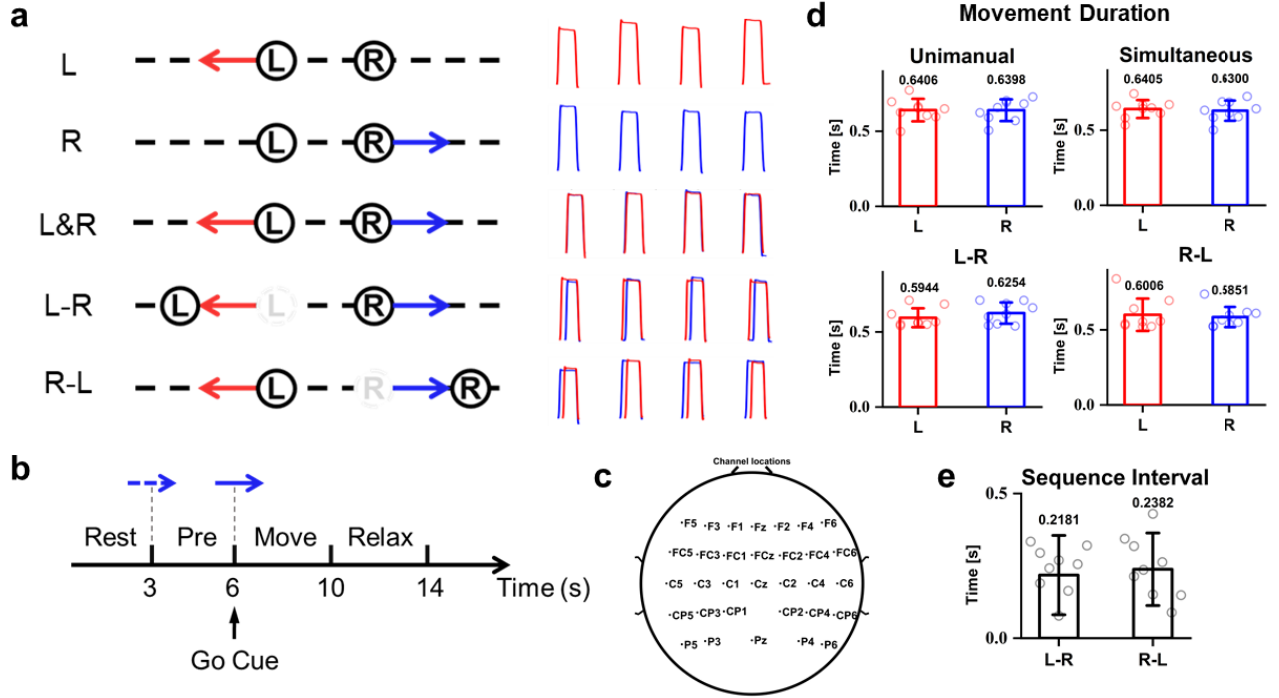
Fig. 1. Illustration of (a) experimental paradigm of different movement tasks and the hand movements' trajectories illustrations. Among these, *L* corresponds to the experiment block of moving the unimanual left hand, *R* corresponds to moving the unimanual right hand, *L&R* corresponds to moving bimanual hands simultaneously, *L-R* corresponds to moving the left hand first and then moving the right hand sequentially, and *R-L* corresponds to moving right hand first and then moving left hand sequentially, (b) timeline setup, (c) EEG channel locations, and behavior analysis of (d) movement duration time and (e) motor element interval time of movement sequence.

nearest-neighbor graph $\mathcal{G}$ with the weight matrix $W \in \mathbb{R}^{N \times N}$. W represents the affinity of edge joining vertices $\mathbf{x}_i$ and $\mathbf{x}_j$ as in (2).

$$W_{ij} = \begin{cases} 1, & \text{if } \mathbf{x}_i \in N(\mathbf{x}_j) \text{or } \mathbf{x}_j \in N(\mathbf{x}_i) \\ 0, & \text{otherwise} \end{cases} \quad (2)$$

$\mathbf{x}_i \in N(\mathbf{x}_j)$ represents $\mathbf{x}_i$ is in the set of k nearest neighbors of $\mathbf{x}_j$. LSDA constructs both a within-class graph $\mathcal{G}_w$ and a between-class graph $\mathcal{G}_b$ to discover both geometrical and discriminant structures of data. Thus, for each data, the neighbor set $N(\mathbf{x}_i)$ contains the subsets $N_w(\mathbf{x}_i)$ and $N_b(\mathbf{x}_i)$. The weight matrices of $\mathcal{G}_w$ and $\mathcal{G}_b$ are W_w and W_b, respectively, and $W = W_w + W_b$.

The objective of sub-manifold mapping is to keep the within-class points of $\mathcal{G}_w$ closer and the between-class points of $\mathcal{G}_b$ farther. Let $\mathbf{y} = [\mathbf{y}_1, \mathbf{y}_2, \cdots, \mathbf{y}_N]^T$ be such a map, and the objective functions can be written as follows:

$$\min \sum_{i,j} (\mathbf{y}_i - \mathbf{y}_j)^2 W_W i, j \quad (3)$$

$$\max \sum_{i,j} (\mathbf{y}_i - \mathbf{y}_j)^2 W_b i, j \quad (4)$$

Supposing the projection $\mathbf{y}^T = \mathbf{a}^T \mathbf{X}$, the objective functions (3) and (4) can be solved as optimal embedding as follows:

$$\mathbf{X}(\alpha L_b + (1-\alpha) W_w) \mathbf{X}^T \mathbf{a} = \lambda \mathbf{X} D_w \mathbf{X}^T \mathbf{a} \quad (5)$$

$$\mathbf{x}_i \to \mathbf{y}_i = A^T \mathbf{x}_i, \quad (6)$$

i.e., we aim to find a projection matrix $\mathbf{A}$ giving the maximum eigenvalue solution to (5). The projection matrix $\mathbf{A} =$ $[\mathbf{a}_1, \mathbf{a}_2, \cdots, \mathbf{a}_d]$, corresponding to the first d largest eigenvalues, $\lambda_1 > \lambda_2 > \cdots > \lambda_d$. In (5), $\alpha \in [0, 1]$ is a penalty factor between the within-class and between-class projection, $L_b = D_b - W_b$ is the Laplacian matrix of $\mathcal{G}_b$, where D_b is the column sum of W_b, and D_w is the column sum of W_w.

After features mapped into a low-dimensional sub-manifold, we applied the LDA classifier for movement decoding. Five nearest neighbors were set for manifold learning. The classification performance was evaluated using 10×5 cross-validation.

III. RESULTS

A. Behavior Analysis

To unify the neural correlating results with motor behavior, we analyzed the movement duration time for the unimanual, simultaneous bimanual and sequential bimanual movements, and also analyzed the movement interval time between the ending of the first motor element and the start of the second motor element for the sequential bimanual movements, as illustrated in Fig. 1 (d) and (e). For the unimanual and simultaneous bimanual movements, the movement duration time of two hands was similar, and for the sequential bimanual movements, the movement duration time of the first motor element was shorter than that of the second one, though not significant (Wilcoxon signed-rank test). Besides, the movement intervals of L-R and R-L motor sequences were 0.2181 ± 0.1371 s and 0.2382 ± 0.1253 s, respectively. Thus, we could obtain the movement onset time points of the second motor element of the sequence were 0.8125 s and 0.8233 s, respectively, which could be associated with the neural correlating results in the subsequent sections.
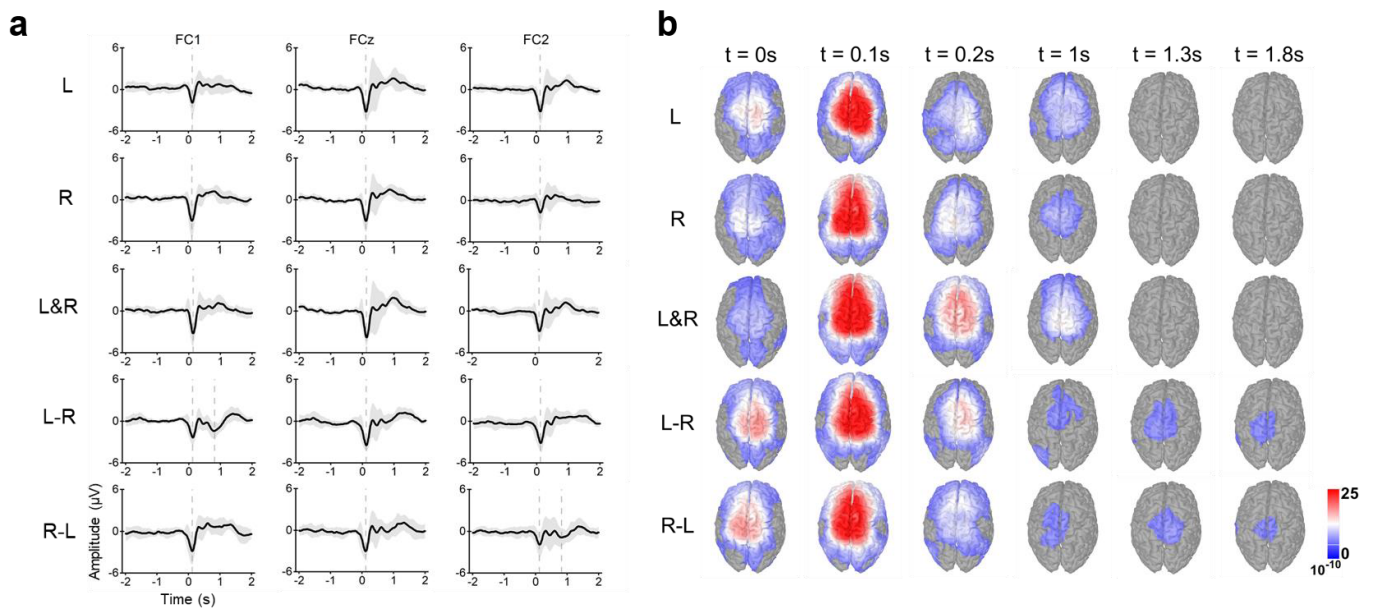
Fig. 2. (a) The movement-related cortical potential (MRCP) plots associated with five movement types. The MRCPs are averaged across all subjects, and the shadows correspond to the deviations. Time 0 s represents the movement onset. (b) The averaged brain activation patterns in source space associated with five movement types. The source-space images are plotted from the top projection view.
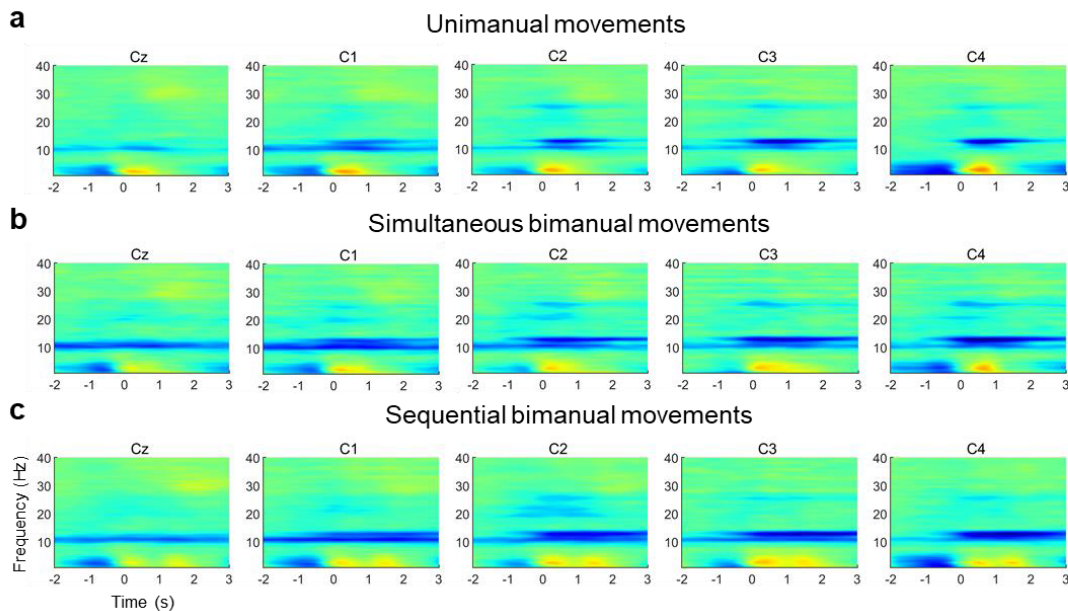

Fig. 3. The time-frequency plots of event-related spectral perturbation (ERSP) for the unimanual, simultaneous bimanual, and sequential bimanual movements.

B. Movement-Related Cortical Potentials (MRCPs)

Fig. 2 (a) depicts the MRCPs in FC1, FCz, and FC2 electrodes under five movement conditions from −2 to 2 s of movement onset. It should be noted that for the sequential movements, the movement onset was calibrated to the first motor sequence element. The MRCPs were plotted at FC1, FCz, and FC2 electrodes because the MRCPs in these channels showed more standard modalities. The MRCPs were averaged across all trials and all subjects, and the shadows corresponded to the deviations across subjects. For all MRCPs, the amplitudes kept steady with a slight negative offset during movement preparation and showed an obvious negative offset before ~200 ms of movement onset and a positive rebound after movement finished. The negative offsets peaked just

after the movement onset and were most prominent in FCz electrode.

For the unimanual movements, contralateral effects were observed with larger negative offsets in the contralateral hemispheres. For the simultaneous bimanual movement, similar negative offsets in bilateral hemispheres were observed. For the sequential bimanual movements, two sequential negative offsets were observed in the contralateral hemisphere of the second motor sequence elements. The negative peaking time of two sequential offsets was in accordance with the movement onset time of two motor elements (according to Fig. 1 (d) and (e)). Wilcoxon signed-rank test showed that there were significant differences of MRCPs between simultaneous bimanual movement (L&R) and sequential bimanual movement (L-R)

at electrode FC1 in [0, 2] s, and also significant differences of MRCPs between simultaneous bimanual movement (L&R) and sequential bimanual movement (R-L) at electrode FC2 in [0, 2] s.

C. EEG Source Images

Fig. 2 (b) presents the brain activation patterns in the source space under different movement conditions. It could be seen that, for all movements, the brain activations were centered on the primary motor cortex, somatosensory cortex, premotor area, and supplementary motor area. For the unimanual movements, stronger activations can be observed in the contralateral hemispheres of motor limbs. Comparing the simultaneous and sequential bimanual movements, we could find that the activations of simultaneous movements were stronger after movement onset, and the activations of sequential movements lasted longer. Besides, the contralateral effects could also be observed for the sequential bimanual movements.

D. Event-Related Oscillations

Fig. 3 shows the time-frequency plots of unimanual, simultaneous bimanual, and sequential bimanual movements. For all movements, a spectral power decrease before movement onset and a power increase after movement onset were observed in the low-frequency band. Compared with the unimanual and simultaneous bimanual movements, two serial low-frequency power increments were observed for the sequential bimanual movements, which were related to the motor sequence. Wilcoxon signed-rank test showed that, for the power sum in the frequency band of [0.01, 4] Hz, there were significant differences between simultaneous bimanual movement and sequential bimanual movement at Electrode Cz in [0, 2] s. The power increment in the low-frequency band could be related to the amplitude's offsets in time domain, and according to Parseval's theorem, the signals' energy in the time domain is equal to that in the frequency domain. Thus, the first power increment in [0, 1] s could be related to the negative offset of movement initiation, as shown in Fig. 2(a) and the second power increment in [1, 2] s could be related to the positive rebound of rest after movement, as shown in Fig. 2(a). Besides, in the alpha band, an obvious event-related desynchronization (ERD) showed for all movements, and it was more prominent and lasted longer time for the sequential bimanual movements compared to others.

E. Discriminating Simultaneous-and-Sequential Bimanual Movements

For both simultaneous and sequential bimanual movements in our experiment, the movement targets of both hands were the same. They represented different ways in which two hands coordinated to reach the same task targets, i.e., left and right hands moving simultaneously (L&R), left and right hands moving sequentially (L-R), and right and left hands moving sequentially (R-L). Thus, we aimed to explore whether the simultaneous and sequential bimanual movements for the same targets could be discriminated against. Fig. 4 (a) gives the continuous decoding results of simultaneous and

sequential bimanual movements using the sliding windows in the pre-movement period and the movement execution period. The decoding windows were shifted from -5 s to -0.5 s in the pre-movement period and from -0.5 s to 3 s in the movement execution period. The length of the window was 1 s, and the step size of the window shift was 0.1 s. Each time point corresponds to the center point of each window. The decoding results were averaged across all subjects. In the pre-movement period, the decoding performance raised from the chance level (0.33 for three-class classification), peaked at around -2.6 s with an accuracy of 50.7%, and then gradually decreased. Similarly, in the movement execution period, the decoding accuracy rose and peaked at 0.5 s with an accuracy of 68.7%. It showed the feasibility of discriminating the simultaneous and sequential bimanual movements both before and after movement onset. Further discussions on the decoding results were given in Section IV.

F. Sequential Movements' Sets and Elements

Planning and executing complex motor skills need the well-organization of motor elements. The sequential bimanual movements in our experiment contained two sequential motor elements of unimanual movements. It meant that the sequential bimanual movement set was comprised of unimanual movement elements, and in the first stage of sequential bimanual movements (L-R and R-L), the motor execution was similar to that of unimanual movements (L and R). Thus, in this section, we aimed to discuss the relationships between the sequential movement sets and elements by comparing the decoding performance between them and also testing the decoding models' generalization ability between them.

Fig. 4 (b) presents the continuous decoding performance comparisons between the unimanual movements (L and R) and the sequential bimanual movements (L-R and R-L) in the pre-movement and movement execution periods. It could be seen that, overall, the binary classification of sequential movements showed better performance, especially in the pre-movement period. In the pre-movement period, the classification of sequential movements peaked at -2.6 s with an accuracy of 70.7%, and the classification of unimanual movements peaked at -2.7 s with an accuracy of 61.3%. In the movement execution period, the classification of sequential movements peaked at 0.5 s with an accuracy of 84.7%, and the classification of unimanual movements peaked at 0.4 s with an accuracy of 81.0%.

Besides, considering the first elements of sequential bimanual movement subsets were the same as unimanual movements, we tested the generalization ability of the models established based on these two motor tasks. For each decoding window, the decoding model trained from the data of unimanual tasks was tested using the data of sequential bimanual tasks, and vice versa. There generalization test from unimanual tasks to sequential bimanual tasks was named GT1 and the opposite generalization test was named GT2. Fig. 4 (c) shows the generalization performance comparisons of the two models. For both models, they showed above-chance-level generalization performance in both pre-movement and motor execution periods. This implied that the unimanual movements

and sequential bimanual movements contained similar motor information, which had been learned by the training models. Besides, in the movement execution period, better generalization performance was obtained for GT1, which suggested the training models established based on unimanual tasks could generalize to sequential bimanual movements better.

G. Visualization of Manifold Learning

For the decoding model, we applied the LSDA method to discover the intrinsic geometrical structure of the underlying data manifold for feature dimension reduction. Specifically, we aimed to find a sub-manifold mapping $\mathbf{y}$ that could keep the within-class points closer and the between-class points farther. To visualize the effectiveness of sub-manifold mapping, we plotted the projected features' scatter plot of one subject using a projection matrix $\mathbf{A}$ with the first two eigenvalues, as shown in Fig. 4 (d). It could be seen that the LSDA found a projection mapping in which the within-class points kept close and the between-class points kept away, especially for the binary classification. Besides, the topographic plots of averaged projection matrixes are presented in Fig. 4 (e). It could be seen that the electrodes in the central, frontal-central, and parietal-central areas were most weighted, related to the cognition of motor task, motor planning and motor execution, indicating the effectiveness of the manifold learning-based feature extraction method.

IV. Discussions and Conclusion

Previous studies have explored bimanual motor BCIs based on EEG signals, including motor tasks of simultaneous bimanual reaching movements, bimanual reach-and-grasp movements, and bimanual motor imagination. However, few studies have focused on the neural correlate and movement decoding of simultaneous-and-sequential bimanual movements. For the same bimanual movement tasks, besides reaching targets using both hands simultaneously, planning and performing motor tasks into sequential motor elements are more natural. Since the reaching targets for both hands can be reached simultaneously or sequentially, the difference in the motor encoding patterns of these two different motor behaviors and whether it is feasible to discriminate them from EEG signals need to be explored.

In this study, we designed an experiment including the unimanual, simultaneous bimanual, and sequential bimanual movements. Neural correlates in the view of the MRCPs, event-related oscillations, and source imaging were done, and a manifold learning-based method was applied for movement decoding. Experimental results suggested unique neural encoding patterns of sequential movements compared to unimanual and simultaneous bimanual movements, especially in low frequency. The simultaneous and sequential bimanual movements were discriminated, and the decoding showed good performance in the pre-movement period, which could be associated with more brain source allocations for the working memory encoding of the motor sequence. Besides, the relationships between motor sequence subsets and elements were discussed.

A. Encoding of Sequential Bimanual Movements

Bimanual coordination is a fundamental motor skill of humans, which involves planning motor behavior ahead of movement initiation, performing motor elements of bimanual movements, and regulating motor behavior dynamically according to real-time neurofeedback. Simultaneous and sequential bimanual movements are two bimanual coordination manners for the same motor task. By the neural correlates, we found the different motor-encoding patterns of simultaneous-and-sequential bimanual movements. For the simultaneous bimanual movement, symmetric activations in bilateral hemispheres were observed, while for the sequential bimanual movements, asymmetric activations with contralateral effects were observed, as shown in Fig. 2. The sequential contralateral activations were associated with the sequential unimanual motor elements. Maximum negative amplitude happened at 0 s in Fig. 2(a), and strongest activation happened at 0.1 s in Fig. 2(b). Considering the MRCPs are time-locked and the calculation of the forward model and inverse estimation in source space are not precise, the strongest neural activation could be seen as happening at 0 s.

In our experiment, sequential bimanual movements contained two sequential unimanual movements. Correspondingly, two sequential spectral power increments in the low frequency were observed in the time-frequency maps (as shown in Fig. 3). Besides, in the MRCP plots, two sequential negative offsets after movement onsets were observed (as shown in Fig. 2 (a)). The sequential negative offsets were only observed in the contralateral electrodes of the second motor element, which were associated with stronger activities in the contralateral hemisphere. For the ipsilateral electrodes of the second motor element, it could be seen that its negative offsets were almost canceled out with the positive rebound associated with the first motor element. Besides, it should be noted that the negative peaking time of the second element was accorded with the movement onset time calculated in Section II. A, which verified the neurophysiological correlates between motor behavior and neural patterns in our study.

B. Decoding Simultaneous-and-Sequential Bimanual Movements From Pre-Movement Period

In this study, we applied a manifold learning-based method to discriminate the simultaneous-and-sequential bimanual movements. Good continuous decoding performance above chance level was obtained in both pre-movement and movement execution periods. Besides, compared with the classification of unimanual movements, the classification of sequential bimanual movements showed better performance in both pre-movement and movement execution periods. The continuous decoding results in the movement execution periods were in accordance with previous studies on motor BCIs [17], and the better performance of sequential movements could be associated with the stronger difference in brain activities between sequential movements.

For the continuous decoding in the pre-movement period, the good performance of sequential movements' decoding could be attributed to that more brain source was allocated
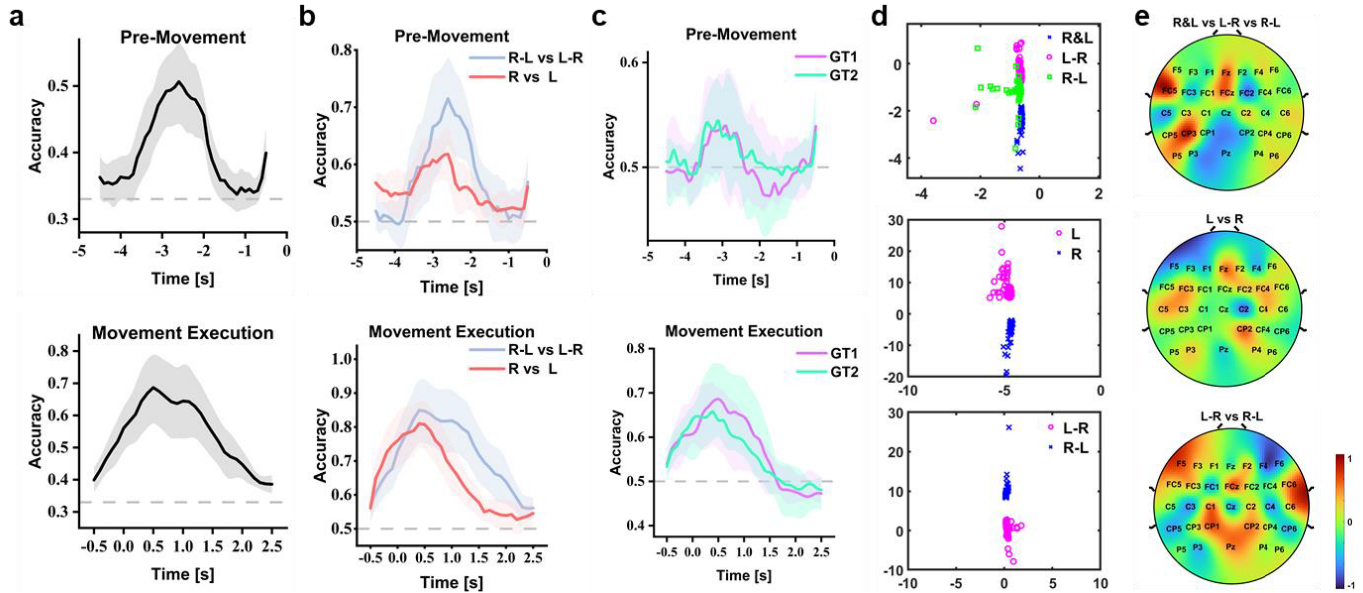
Fig. 4. The decoding performance of movements using the manifold-based decoder. (a) The continuous decoding results of simultaneous and sequential bimanual movements (three-class classifications, R&L vs R-L vs L-R) in both pre-movement and movement execution periods. (b) The decoding comparisons between the unimanual movements and sequential bimanual movements, of which the first motor element was the same with the unimanual movements. (c) Generalization performance comparisons between the unimanual movements and sequential bimanual movements. GT1 represents the generalization test from unimanual tasks to sequential bimanual tasks and GT2 represents the opposite one. (d) One example of scatter plots of sub-manifold mapping using the projection matrix with the first two eigenvalues. (e) Topographic plots of projection matrixes.

for the working memory encoding of a motor sequence. For sequential movements, a person would plan the motor sequence prior to movement execution, instead of planning and executing each motor element of sequence individually and separately. The movement preparation period comprised planning motor sequence and encoding the plan in the working memory. The plan and memory of complex motor sequences would correspond to more brain source allocations, which could result in better decoding performance in the pre-movement period.

C. Relationships Between Motor Set and Motor Element of the Motor Sequence

In our experiment, the motor sequence consisted of two motor elements, i.e., two sequential unimanual movements. Sequential movement requires a well-ordered organization of individual motor elements and was held as a subset in working memory, as opposed to the separate encoding of each individual element [20]. Thus, when developing the decoding model, we regarded the motor sequence as a set. Now, we want to discuss the relationships between motor sequence and its motor elements by the generalization test. The decoding models established using data of sequential movements were tested using data of unimanual movements, i.e., the first motor element of the sequence, and vice versa. Results in Fig. 4 (c) showed the above-chance-level performance in both pre-movement and movement execution periods, which indicated the generalization ability between the motor sequence set and its motor elements. Previous studies in the rhesus monkey also discovered that most neurons within the premotor cortex encoded significant information about only the first or the second motor elements during the working-memory period, and adding new information about the second motor

element would not incur the loss of information about the first motor element [29]. This indicated that the introduction of the second motor element would not corrupt the working memory holding the first motor element, which corresponded to the good generalization ability between models established based on the sequence subset and element in this study.

D. Comparisons With Existing Research

In recent years, decoding bimanual movements from EEG signals has attracted much attention. In 2018, Vuckovic et al. [30] presented a classifier to decode uni-and bi-manual MI with features based on band common spatial patterns and band specifics common spatial patterns. In 2020, Schwarz et al. [15] utilized the low-frequency time-domain feature and shrinkage linear discriminant analysis classifier to discriminate the unimanual and bimanual reach-and-grasp actions with 7-class-classification accuracies of 38.6 ± 6.6%. Besides, in our previous work, we discriminated unimanual and bimanual movements' directions with temporal feature and support vector machine classifier, and six-class classification accuracy reached 70.29%± 10.85% [17]. Different from previous studies, we discriminated different bimanual coordination movements from EEG signals in this study. Using LSDA to extract embedded temporal features and LDA classifier, three-class accuracy reached an average of 68.7%. It should be noted that comparing decoding accuracies across studies directly is not fair because there are differences in experimental paradigms, participants, signals collection devices, decoding methods, etc. Apart from decoding methods, this work is more valuable because it is the first study to correlate and decode different bimanual coordination movements of the same task target from EEG signals.

E. Limitations and Future Work

In this work, we studied the simultaneous-and-sequential bimanual movements for the same task targets. Though we compared the neural correlates of simultaneous-and-sequential bimanual movements, discriminated the bimanual movements, and also discussed the generalization relationships between the motor subset and elements, some further work could be dedicated to the following directions.

In our experiment, we designed the bimanual motor sequence that consisted of two sequential unimanual movements, and more complex motor sequences that consisted of more motor elements could be studied in the future to study their encoding patterns and decoding performance. Besides, in this study, the simultaneous-and-sequential bimanual movements in reaching tasks were explored as preliminary work, and more tasks in real application scenarios can be explored in the future. Besides, more basic works about the neural correlates of simultaneous and sequential bimanual movements could be built upon. Up to now, the neural correlates and movement decoding were analyzed using offline data. In future work, an online test with two manipulators could be done to develop a more natural bimanual-coordination BCI for neurorehabilitation and daily assistance, and intelligent assistive technologies could be introduced to enhance the online performance [31].

REFERENCES

[1] J. D. R. Millán, "Combining brain–computer interfaces and assistive technologies: State-of-the-art and challenges," *Frontiers Neurosci.*, vol. 1, Sep. 2010, Art. no. 161.

[2] M. A. Khan, R. Das, H. K. Iversen, and S. Puthusserypady, "Review on motor imagery based BCI systems for upper limb post-stroke neurorehabilitation: From designing to application," *Comput. Biol. Med.*, vol. 123, Aug. 2020, Art. no. 103843.

[3] J. R. Wolpaw et al., "An EEG-based brain–computer interface for cursor conrol," *Electroencephalogr. Clin. Neurophysiol.*, vol. 78, no. 3, pp. 252–259, Mar. 1991.

[4] L. Pan et al., "Riemannian geometric and ensemble learning for decoding cross-session motor imagery electroencephalography signals," *J. Neural Eng.*, vol. 20, no. 6, Dec. 2023, Art. no. 066011.

[5] Z. Wang et al., "Motor imagery and action observation induced electroencephalographic activations to guide subject-specific training paradigm: A pilot study," *IEEE Trans. Neural Syst. Rehabil. Eng.*, vol. 31, pp. 2457–2467, 2023.

[6] N. Cheng et al., "Brain-computer interface-based soft robotic glove rehabilitation for stroke," *IEEE Trans. Biomed. Eng.*, vol. 67, no. 12, pp. 3339–3351, Dec. 2020.

[7] G. R. Müller-Putz et al., "Applying intuitive EEG-controlled grasp neuroprostheses in individuals with spinal cord injury: Preliminary results from the MoreGrasp clinical feasibility study," in *Proc. 41st Annu. Int. Conf. IEEE Eng. Med. Biol. Soc. (EMBC)*, Jul. 2019, pp. 5949–5955.

[8] N. Robinson, C. Guan, A. P. Vinod, K. K. Ang, and K. P. Tee, "Multi-class EEG classification of voluntary hand movement directions," *J. Neural Eng.*, vol. 10, no. 5, Oct. 2013, Art. no. 056018.

[9] B. Peng, L. Bi, Z. Wang, A. G. Feleke, and W. Fei, "Robust decoding of upper-limb movement direction under cognitive distraction with invariant patterns in embedding manifold," *IEEE Trans. Neural Syst. Rehabil. Eng.*, vol. 32, pp. 1344–1354, 2024.

[10] M. Nann et al., "Restoring activities of daily living using an EEG/EOG-controlled semiautonomous and mobile whole-arm exoskeleton in chronic stroke," *IEEE Syst. J.*, vol. 15, no. 2, pp. 2314–2321, Jun. 2021.

[11] R. Rupp, M. Rohm, M. Schneiders, A. Kreilinger, and G. R. Müller-Putz, "Functional rehabilitation of the paralyzed upper extremity after spinal cord injury by noninvasive hybrid neuroprostheses," *Proc. IEEE*, vol. 103, no. 6, pp. 954–968, Jun. 2015.

[12] G. Pfurtscheller, T. Solis-Escalante, R. Ortner, P. Linortner, and G. R. Müller-Putz, "Self-paced operation of an SSVEP-based orthosis with and without an imagery-based 'brain switchs a feasibility study towards a hybrid BCI," *IEEE Trans. Neural Syst. Rehabil. Eng.*, vol. 18, no. 4, pp. 409–414, Aug. 2010.

[13] R. Foong et al., "Assessment of the efficacy of EEG-based MI-BCI with visual feedback and EEG correlates of mental fatigue for upper-limb stroke rehabilitation," *IEEE Trans. Biomed. Eng.*, vol. 67, no. 3, pp. 786–795, Mar. 2020.

[14] K. Nakayashiki, M. Saeki, Y. Takata, Y. Hayashi, and T. Kondo, "Modulation of event-related desynchronization during kinematic and kinetic hand movements," *J. NeuroEng. Rehabil.*, vol. 11, no. 1, May 2014, Art. no. 90.

[15] A. Schwarz, J. Pereira, R. Kobler, and G. R. Müller-Putz, "Unimanual and bimanual reach-and-grasp actions can be decoded from human EEG," *IEEE Trans. Biomed. Eng.*, vol. 67, no. 6, pp. 1684–1695, Jun. 2020.

[16] A. N. Belkacem, S. Nishio, T. Suzuki, H. Ishiguro, and M. Hirata, "Neuromagnetic decoding of simultaneous bilateral hand movements for multidimensional brain–machine interfaces," *IEEE Trans. Neural Syst. Rehabil. Eng.*, vol. 26, no. 6, pp. 1301–1310, Jun. 2018.

[17] J. Wang, L. Bi, W. Fei, and C. Guan, "Decoding single-hand and both-hand movement directions from noninvasive neural signals," *IEEE Trans. Biomed. Eng.*, vol. 68, no. 6, pp. 1932–1940, Jun. 2021.

[18] J. Wang, L. Bi, A. G. Feleke, and W. Fei, "MRCPs-and-ERS/D-oscillations-driven deep learning models for decoding unimanual and bimanual movements," *IEEE Trans. Neural Syst. Rehabil. Eng.*, vol. 31, pp. 1384–1393, 2023.

[19] Y.-C. Jiang et al., "Characterization of bimanual cyclical tasks from single-trial EEG-fNIRS measurements," *IEEE Trans. Neural Syst. Rehabil. Eng.*, vol. 30, pp. 146–156, 2022.

[20] I. Nambu, N. Hagura, S. Hirose, Y. Wada, M. Kawato, and E. Naito, "Decoding sequential finger movements from preparatory activity in higher-order motor regions: A functional magnetic resonance imaging multi-voxel pattern analysis," *Eur. J. Neurosci.*, vol. 42, no. 10, pp. 2851–2859, Nov. 2015.

[21] W. Yi et al., "EEG oscillatory patterns and classification of sequential compound limb motor imagery," *J. NeuroEng. Rehabil.*, vol. 13, no. 1, Jan. 2016, Art. no. 11.

[22] M. Seeber, R. Scherer, and G. R. Müller-Putz, "EEG oscillations are modulated in different behavior-related networks during rhythmic finger movements," *J. Neurosci.*, vol. 36, no. 46, pp. 11671–11681, Nov. 2016.

[23] Y. Bian, H. Qi, L. Zhao, D. Ming, T. Guo, and X. Fu, "Improvements in event-related desynchronization and classification performance of motor imagery using instructive dynamic guidance and complex tasks," *Comput. Biol. Med.*, vol. 96, pp. 266–273, May 2018.

[24] A. Delorme and S. Makeig, "EEGLAB: An open source toolbox for analysis of single-trial EEG dynamics including independent component analysis," *J. Neurosci. Methods*, vol. 134, no. 1, pp. 9–21, Mar. 2004.

[25] A. Gramfort, T. Papadopoulo, E. Olivi, and M. Clerc, "OpenMEEG: Opensource software for quasistatic bioelectromagnetics," *Biomed. Eng. OnLine*, vol. 9, no. 1, p. 45, 2010.

[26] R. D. Pascual-Marqui, "Standardized low-resolution brain electromagnetic tomography (sLORETA): Technical details," in *Proc. 12th Meeting Int.-Pharmaco-EEG-Group*, Barcelona, Spain, 2002, pp. 5–12.

[27] D. Cai et al., "Locality sensitive discriminant analysis," in *Proc. 20th Int. Joint Conf. Artif. Intell.*, Hyderabad, India, 2007, pp. 714–719.

[28] C. Lin, B.-H. Wang, N. Jiang, R. Xu, N. Mrachacz-Kersting, and D. Farina, "Discriminative manifold learning based detection of movement-related cortical potentials," *IEEE Trans. Neural Syst. Rehabil. Eng.*, vol. 24, no. 9, pp. 921–927, Sep. 2016.

[29] M. M. Shanechi, R. C. Hu, M. Powers, G. W. Wornell, E. N. Brown, and Z. M. Williams, "Neural population partitioning and a concurrent brain-machine interface for sequential motor function," *Nature Neurosci.*, vol. 15, no. 12, pp. 1715–1722, Dec. 2012.

[30] A. Vuckovic, S. Pangaro, and P. Finda, "Unimanual versus bimanual motor imagery classifiers for assistive and rehabilitative brain computer interfaces," *IEEE Trans. Neural Syst. Rehabil. Eng.*, vol. 26, no. 12, pp. 2407–2415, Dec. 2018.

[31] J. Wang, L. Bi, and W. Fei, "Multitask-oriented brain-controlled intelligent vehicle based on human–machine intelligence integration," *IEEE Trans. Syst., Man, Cybern., Syst.*, vol. 53, no. 4, pp. 2510–2521, Apr. 2023.